Layered Group-Based Chirp Spread Spectrum Modulation: Waveform Design and Performance Analysis

Quantao Yu, Dongxuan He, Zhiping Lu, and Hua Wang, *Member, IEEE*

Abstract—In recent years, long-range (LoRa) has become one of the most prominent low-power wide-area network (LPWAN) technologies for the Internet of Things (IoT), which is based on a proprietary chirp spread spectrum (CSS) modulation (i.e., LoRa modulation). However, with the ever-increasing transmission demands of various IoT applications, the low-data-rate issue of LoRa modulation has become a critical bottleneck for its extensive deployment. To address this issue, we first formulate a unified framework for CSS-based waveform design and propose a novel layered group-based CSS (LGCSS) modulation scheme to achieve much higher spectral efficiency (SE) and data rate, thus accommodating a wider range of IoT applications. The complete transmitter architecture of LGCSS modulation is presented along with both coherent and non-coherent detection methods. Moreover, a comprehensive performance analysis of our proposed scheme is conducted in terms of orthogonality, bit error probability (BEP), and computational complexity. Extensive numerical simulations are conducted to verify the effectiveness of our theoretical analysis and the superiority of our proposed scheme compared to the traditional counterparts.

Index Terms—IoT, LoRa, chirp spread spectrum, waveform design, performance analysis.

I. Introduction

THE rapid development of the Internet of Things (IoT) paves the way towards a fully intelligent society and helps bridge the gap between the virtual and physical world [1]. According to IoT Analytics, there will be over 30 billion IoT devices in countless scenarios by 2025 [2]. In particular, application domains including but not limited to smart city, smart agriculture, environmental monitoring, and intelligent logistics, has promoted the proliferation of low-power wide-area network (LPWAN) technologies characterized by energy-efficient and cost-effective communications [3].

During the past few years, a variety of LPWAN technologies have emerged in both licensed and unlicensed spectrum, reflecting heterogeneous application requirements.[1] For the licensed spectrum, narrowband IoT (NB-IoT) is the most popular technology which has been developed by the 3rd Generation Partnership Project (3GPP) and incorporated in fifth-generation (5G) network [4]. It has become a key enabler for the realization of massive Machine Type Communications (mMTC). For the unlicensed industrial, scientific and medical (ISM) frequency bands, long-range (LoRa) has become the most leading technology with the dedicated LoRaWAN standard which promises ubiquitous connectivity while maintaining flexible deployment and simple management [5]. Until now, supported by its booming ecosystem, LoRa has been widely adopted to address IoT applications with more than 180 network operators in the world [6].

The essence of LoRa technology lies in its physical (PHY) layer based on a proprietary chirp spread spectrum (CSS) modulation. Specifically, there are four configurable parameters in the LoRa PHY layer that are listed as follows [7].

- Carrier frequency (CF). Since LoRa operates in the unlicensed ISM bands (EU868 MHz band, AU915 MHz band, etc.), CF is configured according to the regional regulations.
- Bandwidth (BW). Typical BW values include 125 kHz, 250 kHz and 500 kHz.[2]
- Spreading factor (SF). SF is the most important parameter of LoRa modulation since it determines the processing gain and the number of information bits within each LoRa symbol since the number of orthogonal chirps is $M = 2^{SF}$. A set of quasi-orthogonal SFs ranging from 7 to 12 are adopted by LoRa modulation, which enables multiple received signals to be demodulated at the same time on the same channel.
- Coding rate (CR). CR represents the number of redundancy bits added to data bits to bulid a codeword, ranging from 1 to 4. A simple Hamming code is employed in the LoRa PHY layer with adjustable code rate denoted as $4/(CR + 4)$ [8].

The inherent processing gain of LoRa modulation increases its robustness against noise, interference, and fading, i.e., high

Q. Yu, D. He, and H. Wang are with Beijing Institute of Technology, Beijing 100081, China(e-mails: 3120215432@bit.edu.cn; dongxuan_he@bit.edu.cn; wanghua@bit.edu.cn)

Z. Lu is with Beijing University of Posts and Telecommunications, Beijing 100876, China(e-mail: luzp@cict.com). Z. Lu is also with China Academy of Telecommunications Technology (CATT), Beijing 100191, China

[1]It should be noted that this field is still rapidly evolving with new technologies continuously emerging, and with existing ones being updated regularly.

[2]In fact, different LoRa chips have different bandwidth settings. For example, the SX1272 has three configurable bandwidth values including 125 kHz, 250 kHz and 500 kHz while the SX1276 can be configured in the range of 7.8 kHz to 500 kHz.

TABLE I
OVERVIEW OF CSS-BASED LORA-LIKE MODULATION SCHEMES.

Modulation Scheme	Category	Design Parameters	Design Methods	SE
LoRa [15]	SC-CSS	$(1, 1, M)$	Intra-group Index	$\frac{SF}{M}$
SSK-LoRa [16]	SC-CSS	$(2, 1, M)$	Inter-layer Index Intra-group Index	$\frac{SF+1}{M}$
DCRK-CSS [17]	SC-CSS	$(L, 1, M)$	Inter-layer Index Intra-group Index	$\frac{SF+\log_2 L}{M}$
DO-LoRa [18]	MC-CSS	$(1, 2, \frac{M}{2})$	Inter-group Multiplexing Intra-group Index	$\frac{2(SF-1)}{M}$
GCSS [19]	MC-CSS	$(1, G, \frac{M}{G})$	Inter-group Multiplexing Intra-group Index	$\frac{G(SF-\log_2 G)}{M}$
TDM-LoRa [20]	MC-CSS	$(2, 1, M)$	Inter-layer Multiplexing Intra-group Index	$\frac{2SF}{M}$
DM-TDM-CSS [21]	MC-CSS	$(2, 2, \frac{M}{2})$	Inter-layer Multiplexing Inter-group Multiplexing Intra-group Index	$\frac{2\cdot2(SF-1)}{M}$
FSCSS-IM [22]	MC-CSS	$(1, 1, M)$	Intra-group Index Combination	$\frac{\lfloor\log_2\binom{M}{m}\rfloor}{M}$
FBI-LoRa-I [23]	MC-CSS	$(1, G, \frac{M}{G})$	Inter-group Multiplexing Intra-group Index Combination	$\frac{G\lfloor\log_2\binom{M/G}{m}\rfloor}{M}$
FBI-LoRa-II [23]	MC-CSS	$(1, G, \frac{M}{G})$	Inter-group Index Combination Intra-group Index Combination	$\frac{g\lfloor\log_2\binom{M/G}{m}\rfloor+\lfloor\log_2\binom{G}{g}\rfloor}{M}$
LCSS [24]	MC-CSS	$(L, 1, M)$	Inter-layer Multiplexing Intra-group Index	$\frac{L\cdot SF}{M}$
LDMCSS [24]	MC-CSS	$(L, 2, \frac{M}{2})$	Inter-layer Multiplexing Inter-group Multiplexing Intra-group Index	$\frac{2L(SF-1)}{M}$

energy efficiency (EE), thus making it a suitable candidate to support low power and long range communications. Nonetheless, the usage of CSS inevitably results in low spectral efficiency (SE) and limited data rate [9]. As a matter of fact, the symbol period of LoRa modulation, denoted by T_s, is determined by the configured BW and SF with $T_s = \frac{2^{SF}}{BW}$. Therefore, the data rate of LoRa modulation is given as $R_b = \frac{\log_2 M}{T_s} = BW\frac{SF}{2^{SF}}$. As such, the maximum achievable data rate of LoRa modulation is only 27 kbps (corresponding to $BW = 500$ kHz and $SF = 7$). However, with the rapid growth of IoT applications, like smart building [10], image transmission [11], and industrial IoT [12], [13], the low-data-rate issue of LoRa modulation has become a critical bottleneck for accommodating the ever-increasing transmission demands.

To overcome this weakness, a variety of CSS-based modulation schemes have been proposed in the literature, which can be collectively referred to as LoRa-like modulation schemes. According to the number of chirps used in one modulation symbol, these LoRa-like modulation schemes can be classified into two categories, namely single chirp CSS (SC-CSS) and multiple chirps CSS (MC-CSS) [14]. In general, MC-CSS modulation schemes usually possess higher SEs and enhanced data rates compared to SC-CSS schemes.

A. Related Works and Design Framework

With the implementation of reverse engineering of LoRa PHY layer, Vangelista [15] first gave a rigorous mathematical description of LoRa modulation. Specifically, a set of M orthogonal upchirps are used to represent the modulation symbols where the information bearing elements are the initial

This article has been accepted for publication in IEEE Transactions on Communications. This is the author's version which has not been fully edited and content may change prior to final publication. Citation information: DOI 10.1109/TCOMM.2024.3511707

3

frequency shifts (FSs) of the modulated upchirps. Apart from the original upchirps, a set of M orthogonal downchirps are used in slope-shift-keying LoRa (SSK-LoRa) modulation where $SF + 1$ information bits are carried within each modulation symbol [16]. Moreover, $SF + \log_2 L$ information bits can be carried within each symbol in discrete chirp rate keying CSS (DCRK-CSS) modulation where the index of L available chirp rates is used to encode additional information bits [17]. Since both SSK-LoRa and DCRK-CSS belong to SC-CSS modulation schemes, their improvements of data rates are still quite marginal. By contrast, MC-CSS modulation schemes, which can increase the SE and data rate more significantly, have attracted more attention from researchers. For example, Vangelista *et al.* [18] proposed DO-LoRa (dual orthogonal LoRa) modulation where $2(SF - 1)$ information bits are encoded in each symbol by multiplexing even and odd upchirps. Inspired by this, the authors in [19] proposed GCSS (group-based CSS) modulation by dividing M orthogonal upchirps into G independent groups and multiplexing the corresponding upchirps in different groups to transmit $G(SF - \log_2 G)$ information bits per symbol. Besides, the authors in [20] proposed TDM-LoRa (time domain multiplexed LoRa) modulation by multiplexing the modulated upchirps and modulated downchirps, through which $2SF$ information bits can be transmitted per symbol. Moreover, DM-TDM-CSS modulation has been proposed in [21], which combines the design methods of DO-LoRa and TDM-LoRa, and thus $4(SF-1)$ information bits can be carried within each modulation symbol.

In addition, Hanif and Nguyen [22] proposed a frequency-shift CSS system with index modulation (FSCSS-IM) which can achieve much higher SE than the conventional LoRa modulation by using the index combinations of orthogonal chirps for message representation. In particular, if the index combinations of m chirps out of M chirps are used, the number of information bits that can be carried by each symbol is given as $\lfloor \log_2 \binom{M}{m} \rfloor$. Moreover, the authors in [23] proposed two novel frequency-bin-index LoRa (FBI-LoRa) modulation schemes, called FBI-LoRa-I and FBI-LoRa-II, respectively. Specifically, FBI-LoRa-I combines the design methods of GCSS and FSCSS-IM by dividing the M orthogonal chirps into G independent groups, using the index combinations of m chirps out of $\frac{M}{G}$ orthogonal chirps in each group and multiplexing all the signal components of G groups, thus allowing a total of $G\lfloor \log_2 \binom{M/G}{m} \rfloor$ information bits per symbol. FBI-LoRa-II, however, exploits both the index combinations of g selected groups out of G independent groups and the index combinations of m chirps out of $\frac{M}{G}$ orthogonal chirps in g selected groups, where a total of $g\lfloor \log_2 \binom{M/G}{m} \rfloor + \lfloor \log_2 \binom{G}{g} \rfloor$ information bits can be transmitted per symbol. More recently, the authors in [24] proposed layered CSS (LCSS) modulation and layered dual-mode CSS (LDMCSS) modulation, which utilize multiple layers for multiplexing chirps with different discrete chirp rates. Assuming L different layers, the number of information bits that can be carried by each modulation symbol is $L \cdot SF$ and $2L(SF - 1)$ for LCSS and LDMCSS, respectively.

Inspired by the aforementioned works, we formulate a unified framework for the waveform design of CSS-based LoRa-like modulation schemes which consists of two parts: 1) design parameters (L, G, K) and 2) design methods. More specifically, the design parameters include:

- L: the number of independent layers with different discrete chirp rates.
- G: the number of independent groups in each layer. All the independent groups in each layer constitute a partition of M-dimensional orthogonal signal space.
- N: the number of orthogonal chirps used in each independent group. Specifically, if all the orthogonal chirps in each independent group are utilized, we have $N = \frac{M}{G}$.

Based on this, the design methods, including *multiplexing*, *index*, and *index combination*, can be applied to the chosen design parameters. All the aforementioned LoRa-like modulation schemes can be involved in this framework. For example, the conventional LoRa modulation can be regarded as a specific modulation scheme under this framework with chosen design parameters $(1, 1, M)$ through intra-group index. To facilitate the understanding, Table I summarizes the characteristics of all aforementioned modulation schemes under our proposed design framework.

B. Motivation and Contributions

Against the above background, this paper focuses on the design of new CSS-based modulation schemes to accommodate the ever-increasing transmission demands of heterogeneous IoT applications. To cope with the low-data-rate issue of LoRa modulation and improve its adaptive transmission capabilities, a unified design framework for CSS-based LoRa-like modulation schemes is formulated, which can provide valuable guidelines for the design and implementation of new CSS-based modulation schemes. On the basis of our presented framework, we propose a novel layered group-based CSS (LGCSS) modulation scheme which can fully exploit all design parameters to achieve a more extensive trade-off between EE and SE, thus accommodating various application domains. The main contributions of this paper are summarized as follows.

1) We formulate a unified framework for CSS-based waveform design and summarize the characteristics of most state-of-the-art LoRa-like modulation schemes under this framework. Different from the existing works only relying on one or two design parameters, we propose a novel layered group-based CSS (LGCSS) modulation scheme which can fully exploit all design parameters of the presented framework to achieve higher SE and better flexibility than its traditional counterparts.

2) The complete transmitter architecture of our proposed LGCSS modulation is presented along with both coherent and non-coherent detection methods. More precisely, LGCSS modulation can be regarded as a specific modulation scheme with chosen design parameters $(L, G, \frac{M}{G})$ through inter-layer multiplexing, inter-group multiplexing and intra-group index.

3) A comprehensive performance analysis of our proposed scheme is conducted in terms of orthogonality, bit error

probability (BEP), and computational complexity. Specifically, the orthogonality of our proposed modulation scheme is thoroughly investigated. Based on this, the approximate closed-form BEP expression over additive white Gaussian noise (AWGN) channel is derived, which serves as a lower bound for the exact error probability. In addition, the computational complexities of our proposed modulation scheme and its classical counterparts are analyzed.

4) Extensive numerical simulations are demonstrated to verify the effectiveness of our theoretical analysis and the superiority of our proposed modulation scheme. Specifically, the bit-error-rate (BER) and effective throughput of LGCSS modulation and its traditional counterparts over both AWGN and typical fading channels are demonstrated. Additionally, its BER performance under the impact of phase offset (PO) and frequency offset (FO) is also presented. Moreover, we elucidate the merits and limitations of our proposed modulation scheme and pinpoint some future research directions.

C. Paper Organization and Notations

The remainder of this paper is organized as follows. Section II presents the system model of our proposed LGCSS modulation. Section III is devoted to an overall performance analysis of our proposed scheme. The numerical results are demonstrated and discussed in Section IV. Finally, Section V concludes the whole paper.

Notation: Throughout this paper, we denote $F_X(x)$ and $f_X(x)$ as the cumulative distribution function (CDF) and the probability density function (PDF) of random variable X. $[\cdot]^T$, $(\cdot)^*$, $|\cdot|$, and $\Re\{\cdot\}$ stand for the transpose, conjugate, absolute value, and real part operators. $\mathbb{E}[\cdot]$ and $\Pr\{\cdot\}$ denote the mathematical expectation and probability measure, respectively. $Q(x) = \frac{1}{\sqrt{2\pi}} \int_x^\infty \exp\left(-\frac{u^2}{2}\right) du$ is the Gaussian Q-function.

II. SYSTEM MODEL

In this section, we present the system model of our proposed LGCSS modulation scheme. The complete transmitter architecture is illustrated in Fig. 1.

A. Transmission

Considering LGCSS modulation with design parameters $(L, G, \frac{M}{G})$, a total of $L \cdot S$ information bits can be transmitted within each modulation symbol with $S = G(SF - \log_2 G)$. As depicted in Fig. 1, the operation procedures at the transmitter are presented as follows.

Step 1: The transmitted information bits within each LGCSS modulation symbol are split into L layers where each layer carries S information bits with its own chirp rate (i.e., the frequency slope of the utilized basic chirp).

Specifically, in the discrete-time complex baseband-equivalent form, each chirp can be defined by $M = 2^{SF}$

samples and we denote the basic chirp utilized in the lth layer as $c_l[n]$, given by

$$c_l[n] = \frac{1}{\sqrt{M}} \exp\left\{j\frac{\pi l n^2}{M}\right\}, \tag{1}$$

where $l \in \{1, ..., L\}$ is the layer index and $n = 0, 1, ..., M-1$ is the sample index.

Step 2: The S information bits encoded in each layer are divided into G independent groups and thus the number of information bits carried by each group is $T = SF - \log_2 G$.

Step 3: Every T information bits carried by each group, represented by $\boldsymbol{b^{l,g}} = [b_0^{l,g}, b_1^{l,g}, ..., b_{T-1}^{l,g}]$, are mapped to a data symbol according to the following mapping rule

$$m_g^l = (g-1)\frac{M}{G} + \sum_{i=0}^{T-1} b_i^{l,g} 2^i, \tag{2}$$

where $g \in \{1, ..., G\}$ is the group index and thus m_g^l denotes the data symbol of the gth group in the lth layer.

Step 4: The modulation signal component of the lth layer $s_l[n]$ is obtained through the design methods of intra-group index and inter-group multiplexing, which can be expressed as

$$s_l[n] = \sqrt{\frac{1}{G}} \sum_{g=1}^{G} c_l[n] \exp\left\{j\frac{2\pi m_g^l n}{M}\right\}. \tag{3}$$

Step 5: The transmitted signal of LGCSS modulation $s[n]$ is obtained through the design method of inter-layer multiplexing, which is given as

$$s[n] = \frac{1}{\sqrt{LG}} \sum_{l=1}^{L} \sum_{g=1}^{G} c_l[n] \exp\left\{j\frac{2\pi m_g^l n}{M}\right\}. \tag{4}$$

As such, the SE of LGCSS modulation is given by

$$\eta = \frac{LG(SF - \log_2 G)}{M}. \tag{5}$$

It can be noticed that by exploiting all design parameters including L, G, and M, LGCSS modulation can achieve much higher SE and better flexibility than its traditional counterparts. In particular, LGCSS modulation will fall back to LCSS modulation and GCSS modulation when $G = 1$ and $L = 1$, respectively. Furthermore, the conventional LoRa modulation can also be regarded as a special variant of LGCSS modulation with both L and G equaling to 1.

B. Detection

Assuming ideal synchronization, the received signal in a frequency-flat fading channel, denoted by $r[n]$, is given as

$$r[n] = hs[n] + w[n], \tag{6}$$

where h denotes the complex channel gain with $\mathbb{E}\{|h|^2\} = 1$ and $w[n] \sim \mathcal{CN}(0, \sigma^2)$ is the additive white Gaussian noise. Notably, the channel will be AWGN channel when $h = 1$. Let $\boldsymbol{r} = [r[0], ..., r[M-1]]^T$ and $\boldsymbol{s} = [s[0], ..., s[M-1]]^T$, the optimal maximum likelihood estimation of the transmitted
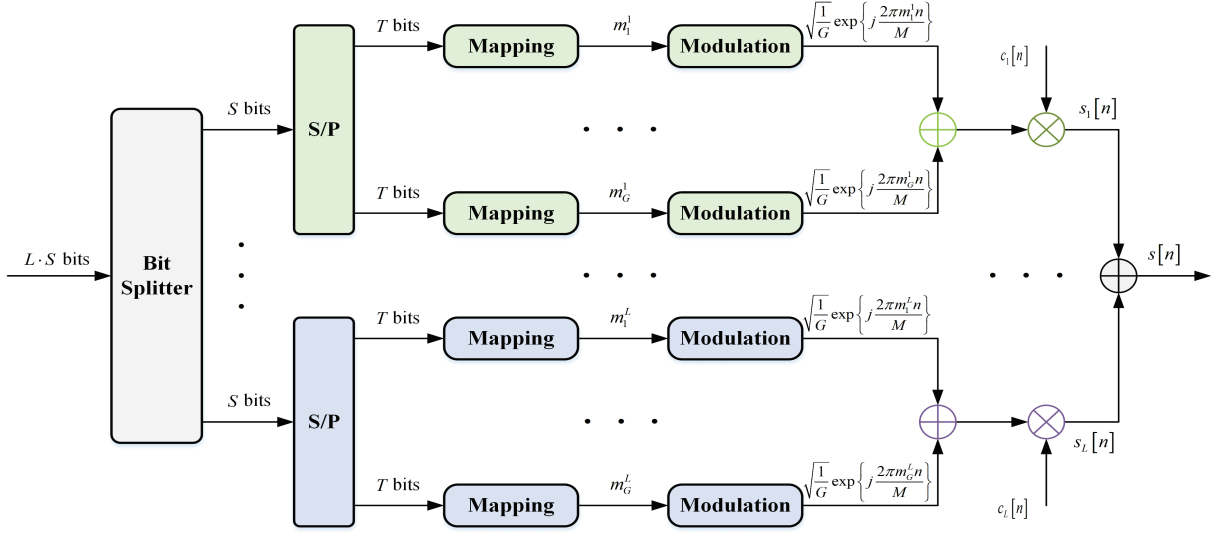
Fig. 1. Transmitter architecture of the proposed LGCSS modulation scheme.

data symbols maximizes the likelihood function given as

$$p(\boldsymbol{r}|\boldsymbol{s}, h) = (\frac{1}{\pi\sigma^2})^M \exp\left\{-\frac{||\boldsymbol{r} - h\boldsymbol{s}||^2}{\sigma^2}\right\}$$
$$= C \exp\left\{\frac{2\Re\left\{h^* \sum_{n=0}^{M-1} r[n]s^*[n]\right\}}{\sigma^2}\right\}, \quad (7)$$

where

$$C = (\frac{1}{\pi\sigma^2})^M \exp\left\{-\frac{||\boldsymbol{r}||^2 + |h|^2 \, ||\boldsymbol{s}||^2}{\sigma^2}\right\} \quad (8)$$

is independent of the transmitted data symbols. Therefore, when the channel state information (i.e., h) is available at the receiver, the optimal coherent detection can be expressed as

$$\left\{\hat{m}_1^l, ..., \hat{m}_G^l\right\}_{l=1}^L = \arg\max \Re\left\{h^* \sum_{n=0}^{M-1} r[n]s^*[n]\right\}. \quad (9)$$

Specifically, for our proposed LGCSS modulation, we have

$$\sum_{n=0}^{M-1} r[n]s^*[n] = \frac{1}{\sqrt{LG}} \sum_{l=1}^L \sum_{g=1}^G \sum_{n=0}^{M-1} r[n]c_l^*[n]$$
$$\times \exp\left\{-j\frac{2\pi m_g^l n}{M}\right\} \quad (10)$$
$$= \frac{1}{\sqrt{LG}} \sum_{l=1}^L \sum_{g=1}^G R_l[k_g],$$

where $R_l[k] = \sum_{g=1}^G R_l[k_g]$ is the M-point discrete Fourier transform (DFT) of $r[n]c_l^*[n]$ with $k_g \in \left\{(g-1)\frac{M}{G}, ..., g\frac{M}{G} - 1\right\}$ representing the frequency bin index of the gth group.

As such, by substituting (10) into (9), the coherent detection can be simplified as

$$\left\{\hat{m}_1^l, ..., \hat{m}_G^l\right\}_{l=1}^L = \arg\max \Re\left\{\frac{h^*}{\sqrt{LG}} \sum_{l=1}^L R_l[k]\right\}. \quad (11)$$

Moreover, the data symbols can be separately detected layer by layer. In particular, consistent with the symbol mapping rule in (2), the gth data symbol in the lth layer can be obtained as

$$\hat{m}_g^l = \arg\max_k \Re\left\{h^* R_l[k]\right\}, k \in \left\{(g-1)\frac{M}{G}, ..., g\frac{M}{G} - 1\right\}. \quad (12)$$

Furthermore, when the receiver does not have the knowledge of h, the non-coherent detection for the gth data symbol in the lth layer can be expressed as

$$\hat{m}_g^l = \arg\max_k |R_l[k]|, k \in \left\{(g-1)\frac{M}{G}, ..., g\frac{M}{G} - 1\right\}. \quad (13)$$

As a result, both coherent and non-coherent detection keep the similar methodology to that of the traditional counterparts, which can be divided into three steps, i.e., dechirp, DFT, and frequency domain (FD) peak index decision [19].

Remark 1: In practice, accurate channel state information (CSI) is required for coherent detection at the receiver, where channel estimation is necessary before symbol detection. However, channel estimation will increase the receiver's complexity, thus making coherent detection impractical for resource-limited low-cost IoT devices. From the implementation point of view, coherent detection is less desirable than non-coherent detection that can operate without CSI in the context of LPWAN communications. Therefore, we only consider non-coherent detection for performance analysis and numerical simulations in the sequel.

III. PERFORMANCE ANALYSIS

In this section, a comprehensive performance analysis of our proposed LGCSS modulation is conducted in terms of orthogonality, BEP, and computational complexity.

A. Orthogonality Analysis

To investigate the orthogonality of our proposed LGCSS modulation scheme, we consider the inner product of two

distinct modulation symbols $\boldsymbol{s} = [s[0], ..., s[M-1]]^T$ and $\widetilde{\boldsymbol{s}} = [\widetilde{s}[0], ..., \widetilde{s}[M-1]]^T$ as $\langle \boldsymbol{s}, \widetilde{\boldsymbol{s}} \rangle = \sum_{n=0}^{M-1} s[n]\widetilde{s}^*[n]$, where $\langle \cdot, \cdot \rangle$ represents the inner product operation. Without loss of generality, we define m_g^l as the g-th data symbol in the l-th layer of $\boldsymbol{s}$ and $\tilde{m}_{\widetilde{g}}^{\widetilde{l}}$ as the $\widetilde{g}$-th data symbol in the $\widetilde{l}$-th layer of $\widetilde{\boldsymbol{s}}$, where $g, \widetilde{g} \in \{1, ..., G\}$ and $l, \widetilde{l} \in \{1, ..., L\}$. Considering the same layer of $\boldsymbol{s}$ and $\widetilde{\boldsymbol{s}}$, i.e., $l = \widetilde{l}$, we have $m_g^l \neq \tilde{m}_{\widetilde{g}}^{\widetilde{l}}$ for $g = \widetilde{g}$.

As such, for the proposed LGCSS modulation, the inner product can be given as

$$\langle \boldsymbol{s}, \widetilde{\boldsymbol{s}} \rangle = \frac{1}{L} \sum_{l=1}^{L} \sum_{\widetilde{l}=1}^{L} \sum_{n=0}^{M-1} s_l[n]\widetilde{s}_{\widetilde{l}}^*[n] = \frac{1}{L} \sum_{l=1}^{L} \sum_{\widetilde{l}=1}^{L} \langle \boldsymbol{s_l}, \widetilde{\boldsymbol{s}_{\widetilde{l}}} \rangle, \tag{14}$$

where

$$\langle \boldsymbol{s_l}, \widetilde{\boldsymbol{s}_{\widetilde{l}}} \rangle = \frac{1}{GM} \sum_{g=1}^{G} \sum_{\widetilde{g}=1}^{G} \sum_{n=0}^{M-1} \exp\left\{ j\frac{\pi\alpha_{(l,\widetilde{l})}n^2}{M} \right\} \times \exp\left\{ j\frac{2\pi\beta_{(m_g^l, \tilde{m}_{\widetilde{g}}^{\widetilde{l}})}n}{M} \right\}, \tag{15}$$

with $1 - L \leq \alpha_{(l,\widetilde{l})} = l - \widetilde{l} \leq L - 1$, $\beta_{(m_g^l, \tilde{m}_{\widetilde{g}}^{\widetilde{l}})} = m_g^l - \tilde{m}_{\widetilde{g}}^{\widetilde{l}}$. It can be observed that the orthogonality of our proposed modulation scheme relies on the parameter $\alpha_{(l,\widetilde{l})}$. Therefore, to obtain the general expressions regarding the orthogonality of our proposed scheme, two different cases should be evaluated, namely, (i) $\alpha_{(l,\widetilde{l})} = 0$, i.e., $l = \widetilde{l}$ and (ii) $\alpha_{(l,\widetilde{l})} \neq 0$, i.e., $l \neq \widetilde{l}$.

Case I: In this case, the inner product $\langle \boldsymbol{s_l}, \widetilde{\boldsymbol{s}_{\widetilde{l}}} \rangle$ is given as

$$\langle \boldsymbol{s_l}, \widetilde{\boldsymbol{s}_{\widetilde{l}}} \rangle = \frac{1}{GM} \sum_{g=1}^{G} \sum_{\widetilde{g}=1}^{G} \sum_{n=0}^{M-1} \exp\left\{ j\frac{2\pi(m_g^l - \tilde{m}_{\widetilde{g}}^{\widetilde{l}})n}{M} \right\} = 0. \tag{16}$$

Hence, we have $\langle \boldsymbol{s}, \widetilde{\boldsymbol{s}} \rangle = 0$ in this case.

Case II: In this case, the inner product $\langle \boldsymbol{s_l}, \widetilde{\boldsymbol{s}_{\widetilde{l}}} \rangle$ is given as

$$\langle \boldsymbol{s_l}, \widetilde{\boldsymbol{s}_{\widetilde{l}}} \rangle = \frac{1}{GM} \times \sum_{g=1}^{G} \sum_{\widetilde{g}=1}^{G} \underbrace{\sum_{n=0}^{M-1} \exp\left\{ j\frac{\pi}{M}[\alpha_{(l,\widetilde{l})}n^2 + 2\beta_{(m_g^l, \tilde{m}_{\widetilde{g}}^{\widetilde{l}})}n] \right\}}_{I_{m_g^l, \tilde{m}_{\widetilde{g}}^{\widetilde{l}}}^{l,\widetilde{l}}}, \tag{17}$$

where $I_{m_g^l, \tilde{m}_{\widetilde{g}}^{\widetilde{l}}}^{l,\widetilde{l}}$ can be computed as

$$I_{m_g^l, \tilde{m}_{\widetilde{g}}^{\widetilde{l}}}^{l,\widetilde{l}} = \sqrt{\frac{M}{|\alpha_{(l,\widetilde{l})}|}} \mathcal{A}_{(l,\widetilde{l})}(1 + \mathcal{B}_{(m_g^l, \tilde{m}_{\widetilde{g}}^{\widetilde{l}})}), \tag{18}$$

where

$$\mathcal{A}_{(l,\widetilde{l})} = \exp\left\{ j\frac{\pi|\alpha_{(l,\widetilde{l})}|}{4\alpha_{(l,\widetilde{l})}} \right\} \exp\left\{ -j\frac{\pi\beta_{(m_g^l, \tilde{m}_{\widetilde{g}}^{\widetilde{l}})}^2}{\alpha_{(l,\widetilde{l})}M} \right\}, \tag{19}$$

$$\mathcal{B}_{(m_g^l, \tilde{m}_{\widetilde{g}}^{\widetilde{l}})} = \sum_{n=1}^{|\alpha_{(l,\widetilde{l})}|-1} \exp\left\{ -j\frac{\pi}{\alpha_{(l,\widetilde{l})}}[Mn^2 + 2\beta_{(m_g^l, \tilde{m}_{\widetilde{g}}^{\widetilde{l}})}n] \right\}. \tag{20}$$

The detailed derivation is presented in Appendix A. Therefore, the general expression of inner product $\langle \boldsymbol{s}, \widetilde{\boldsymbol{s}} \rangle$ is given by

$$\langle \boldsymbol{s}, \widetilde{\boldsymbol{s}} \rangle = \frac{1}{LGM} \sum_{l=1}^{L} \sum_{\substack{\widetilde{l}=1 \\ \widetilde{l} \neq l}}^{L} \sum_{g=1}^{G} \sum_{\widetilde{g}=1}^{G} \sqrt{\frac{M}{|\alpha_{(l,\widetilde{l})}|}} \mathcal{A}_{(l,\widetilde{l})}(1 + \mathcal{B}_{(m_g^l, \tilde{m}_{\widetilde{g}}^{\widetilde{l}})}), \tag{21}$$

which indicates the orthogonality is not preserved in this case and thus results in unavoidable interference during the symbol detection.

According to the above orthogonality analysis, the interference during the symbol detection can be quantitatively determined. In particular, the received signal over AWGN channel can be explicitly expressed as

$$r[n] = \frac{1}{\sqrt{LG}} \sum_{l=1}^{L} \sum_{g=1}^{G} c_l[n] \exp\left\{ j\frac{2\pi m_g^l n}{M} \right\} + w[n]. \tag{22}$$

Since the data symbols are separately detected layer by layer, we consider the symbol detection of the $\bar{l}$-th layer without loss of generality. Specifically, the dechirped signal $r_{\bar{l}}[n] = r[n]c_{\bar{l}}^*[n]$ can be expressed as

$$r_{\bar{l}}[n] = \frac{1}{\sqrt{LGM}} \sum_{g=1}^{G} \exp\left\{ j\frac{2\pi m_g^{\bar{l}} n}{M} \right\} + \frac{1}{\sqrt{LGM}} \sum_{\substack{l=1 \\ l \neq \bar{l}}}^{L} \sum_{g=1}^{G} \exp\left\{ j\frac{\pi\alpha_{(l,\bar{l})}n^2}{M} \right\} \times \exp\left\{ j\frac{2\pi m_g^l n}{M} \right\} + \bar{w}[n], \tag{23}$$

where $\bar{w}[n] = w[n]c_{\bar{l}}^*[n] \sim \mathcal{CN}(0, \frac{\sigma^2}{M})$.

Then, the M-point DFT of the dechirped signal can be calculated as

$$R_{\bar{l}}[k] = \sum_{n=0}^{M-1} r_{\bar{l}}[n] \exp\left\{ -j\frac{2\pi kn}{M} \right\}$$
$$= \frac{1}{\sqrt{LGM}} \sum_{g=1}^{G} \sum_{n=0}^{M-1} \exp\left\{ j\frac{2\pi(m_g^{\bar{l}} - k)n}{M} \right\} + \bar{W}[k]$$
$$+ \frac{1}{\sqrt{LGM}} \sum_{g=1}^{G} \sum_{\substack{l=1 \\ l \neq \bar{l}}}^{L} \sum_{n=0}^{M-1} \exp\left\{ j\frac{\pi\alpha_{(l,\bar{l})}n^2}{M} \right\}$$
$$\times \exp\left\{ j\frac{2\pi\beta_{(m_g^l, k)}n}{M} \right\}$$
$$= \frac{1}{\sqrt{LG}} \sum_{g=1}^{G} \delta[k - m_g^{\bar{l}}] + \bar{W}[k]$$
$$+ \frac{1}{\sqrt{LGM}} \sum_{g=1}^{G} \sum_{\substack{l=1 \\ l \neq \bar{l}}}^{L} I_{m_g^l, k}^{l,\bar{l}}, \tag{24}$$

where $\delta[\cdot]$ represents the Kronecker delta function, $\bar{W}[k] = $

$\sum_{n=0}^{M-1} \bar{w}[n] \exp\left\{-j\frac{2\pi kn}{M}\right\} \sim \mathcal{CN}(0, \sigma^2)$.

Since the symbol detection is performed separately for each independent group, we focus on the $\bar{g}$-th group in the $\bar{l}$-th layer. As a result, (24) can be further simplified as

$$R_{\bar{l}}[k] = \underbrace{\frac{1}{\sqrt{LG}}\delta[k - m_{\bar{g}}^{\bar{l}}]}_{\text{signal term}} + \underbrace{\frac{1}{\sqrt{LGM}}\sum_{\substack{l=1 \\ l\neq\bar{l}}}^{L} I_{m_{\bar{g}}^l, k}^{l,\bar{l}}}_{\text{interference term}} + \underbrace{\bar{W}[k]}_{\text{noise term}},$$

$$(25)$$

where $k \in \left\{(\bar{g}-1)\frac{M}{G}, ..., \bar{g}\frac{M}{G} - 1\right\}$. Therefore, the signal-to-interference-plus-noise ratio (SINR) can be calculated as

$$\Gamma = \frac{\mathbb{E}[|\frac{1}{\sqrt{LG}}\delta[k - m_{\bar{g}}^{\bar{l}}]|^2]}{\mathbb{E}[|\frac{1}{\sqrt{LGM}}\sum_{\substack{l=1 \\ l\neq\bar{l}}}^{L} I_{m_{\bar{g}}^l, k}^{l,\bar{l}} + \bar{W}[k]|^2]}$$

$$= \frac{\frac{1}{LG}}{\frac{1}{LGM^2}\mathbb{E}[|\sum_{\substack{l=1 \\ l\neq\bar{l}}}^{L} I_{m_{\bar{g}}^l, k}^{l,\bar{l}}|^2] + \sigma^2}.$$

$$(26)$$

B. BEP Analysis

From (25) one can observe that it's very challenging to derive the exact BEP expression of the proposed modulation scheme due to the interference term. To this end, we first derive the closed-form BEP expression of GCSS modulation. Based on this, the approximate BEP expression of our proposed scheme is obtained, which serves as a lower bound for the exact error probability.[3]

Specifically, the symbol error probability (SEP) of LoRa modulation considering non-coherent detection over AWGN channel is given as [25]

$$P_L^s(M, \gamma_s) = \sum_{k=1}^{M-1} \frac{(-1)^{k+1}}{k+1}\binom{M-1}{k}\exp\left\{-\frac{k}{k+1}\gamma_s\right\},$$

$$(27)$$

where $\gamma_s = 1/\sigma^2$ represents the effective signal-to-noise ratio (SNR). Moreover, its closed-form approximation is given by [26]

$$P_L^s(M, \gamma_s) \approx Q\left(\frac{\sqrt{\gamma_s} - (H_{M-1}^2 - \frac{\pi^2}{12})^{\frac{1}{4}}}{\sqrt{H_{M-1} - (H_{M-1}^2 - \frac{\pi^2}{12})^{\frac{1}{2}} + 0.5}}\right),$$

$$(28)$$

where $H_N = \sum_{i=1}^{N}\frac{1}{i}$ is the Nth harmonic number. It can be observed that P_L^s is a function of γ_s and M. For the detailed derivation of (28), interested readers are referred to [26].

Based on this, the closed-form BEP expression for GCSS modulation can be derived as

$$P_G^b = \frac{M}{2(M-G)}P_L^s\left(\frac{M}{G}, \frac{\gamma_s}{G}\right),$$

$$(29)$$

which in fact is the BEP for an $\frac{M}{G}$-ary orthogonal modulation with the effective SNR becoming $\frac{\gamma_s}{G}$ since the total transmission power is equally allocated to each independent group while the number of orthogonal chirps becomes $\frac{M}{G}$ for each

[3]Note that the BEP analysis here only considers the case of an AWGN channel for simplicity. Nevertheless, the derivation can be easily extended to the case of a fading channel by taking the channel's statistical property into consideration.

group. Notably, P_G^b is a function of γ_s, M and G, which coincides with the design parameters of GCSS modulation. The detailed derivation of (29) is presented in Appendix B.

For LGCSS modulation, although the total transmission power is still equally allocated to each group and the number of orthogonal chirps is also $\frac{M}{G}$ for each group, interference occurs during the symbol detection due to the loss of orthogonality. Therefore, it's hard to obtain the exact closed-form BEP for LGCSS modulation directly. To derive the approximate BEP expression of our proposed LGCSS modulation, we note that the interference term in (25) is inversely proportional to M. As $M \to \infty$, we have

$$\Gamma \leq \Gamma^u = \frac{\frac{1}{LG}}{\sigma^2}.$$

$$(30)$$

Hence, the approximate BEP expression of LGCSS modulation can be obtained as

$$P_{LG}^b \approx \frac{M}{2(M-G)}P_L^s\left(\frac{M}{G}, \frac{\gamma_s}{LG}\right),$$

$$(31)$$

where the effective SNR is approximated as $\frac{\gamma_s}{LG}$ by neglecting the impact of interference. Note that P_{LG}^b is a function of γ_s, L, M and G, which also coincides with the design parameters of LGCSS modulation. Moreover, the derived P_{LG}^b serves as a lower bound for the exact BEP and its tightness can be guaranteed and the performance gap between accurate and approximate BEP will get negligible especially for large M. This is usually reasonable for CSS-based LoRa-like modulation schemes since $M = 2^{SF}$ with SF ranging from 7 to 12.

C. Complexity Analysis

Since most IoT devices are considered to be resource-constrained, computational complexity is one of the crucial aspects that need to be carefully evaluated. Without loss of generality, the demodulation complexity of our proposed modulation scheme can be expressed in the number of required real multiplications (MUL), real additions (ADD), and comparisons (CMP) [27], [39]. For convenience, Table II presents a comprehensive comparison of the computational complexities regarding non-coherent detection of the conventional LoRa, GCSS, LCSS, and our proposed LGCSS modulation.

As mentioned earlier, the symbol detection can be divided into three steps, namely, dechirp, DFT, and FD peak index decision. The MUL and ADD arise from the dechirp and DFT operations. In addition, the CMP arises from the FD peak index decision. Since the main computational complexity arises from the dechirp and DFT operations, it can be observed that the computational complexity is quite similar for LoRa modulation and GCSS modulation in the order of $\mathcal{O}(M\log_2 M)$ since both of them have one dechirp and one DFT operations as a result of the single-layer signal structure. Likewise, LCSS modulation and LGCSS modulation also have similar complexity in the order of $\mathcal{O}(LM\log_2 M)$ since both of them have L dechirp and L DFT operations due to the layered-multiplexing signal structure. Moreover, to measure the complexity for one single transmitted information bit, we define the normalized computational complexity as the number

This article has been accepted for publication in IEEE Transactions on Communications. This is the author's version which has not been fully edited and content may change prior to final publication. Citation information: DOI 10.1109/TCOMM.2024.3511707

8

TABLE II
COMPUTATIONAL COMPLEXITIES OF THE CONSIDERED MODULATION SCHEMES.

Modulation Scheme	Dechirp	DFT	FD Peak Index Decision	Normalized Complexity
LoRa	MUL: $4M$ ADD: $2M$	MUL: $2M\log_2 M$ ADD: $3M\log_2 M$	CMP: $M-1$	$\dfrac{2M(2+\log_2 M)}{SF}$
GCSS	MUL: $4M$ ADD: $2M$	MUL: $2M\log_2 M$ ADD: $3M\log_2 M$	CMP: $G\left(\dfrac{M}{G}-1\right)$	$\dfrac{2M(2+\log_2 M)}{G(SF-\log_2 G)}$
LCSS	MUL: $4LM$ ADD: $2LM$	MUL: $2LM\log_2 M$ ADD: $3LM\log_2 M$	CMP: $L(M-1)$	$\dfrac{2M(2+\log_2 M)}{SF}$
LGCSS	MUL: $4LM$ ADD: $2LM$	MUL: $2LM\log_2 M$ ADD: $3LM\log_2 M$	CMP: $LG\left(\dfrac{M}{G}-1\right)$	$\dfrac{2M(2+\log_2 M)}{G(SF-\log_2 G)}$

of MUL required for each transmitted information bit and summarize the corresponding results in the last column of Table II. Intriguingly, it can be observed that both GCSS modulation and LGCSS modulation have lower normalized complexity than LoRa modulation and LCSS modulation. In other words, GCSS modulation and LGCSS modulation can make a more efficient usage of the computational resources due to the grouped-multiplexing signal structure.

IV. NUMERICAL RESULTS AND DISCUSSIONS

In this section, numerical simulations are conducted to provide an overall performance evaluation of our proposed modulation scheme. We compare the BER and effective throughput of our proposed modulation scheme with that of the conventional LoRa modulation [15], GCSS modulation [19], and LCSS modulation [24] over AWGN and typical fading channels including Rayleigh and Rician fading channels. Unless otherwise specified, we set $SF = 11$ and $BW = 125$ kHz for comparison. Moreover, the energy efficiency (EE) is defined as the required E_b/N_0 for a target BER level.

A. Comparison of Theoretical and Simulation Results

Fig. 2 shows a comparison of theoretical BEP and simulated BER curves of our proposed LGCSS modulation for $SF = 9$ and $SF = 11$ over AWGN channels. The notations "Th." and "Sim." denote the theoretical and simulation results, respectively. Without loss of generality, we set $L = 2$ and $G = 2$. It can be seen that the simulation results agree well with our theoretical analysis in Section III-B. Specifically, the theoretical BEP curves serve as lower bounds for the simulated BER curves. Moreover, due to the loss of orthogonality, a performance gap between the theoretical and simulated curves can be observed. Specifically, for $SF = 9$, the performance gap is around 0.5 dB at a target BER level of 10^{-5}. Nonetheless, the performance gap becomes negligible for $SF = 11$, which shows that the approximated BEP given in (31) serves as a tight lower bound for large M and this substantially verifies the accuracy of our theoretical analysis.
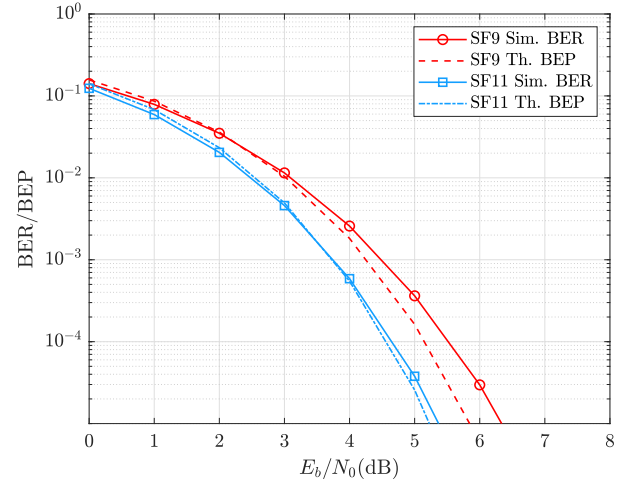

Fig. 2. A comparison of theoretical BEP and simulated BER curves of LGCSS modulation for $SF = 9$ and $SF = 11$ over AWGN channels.

B. BER and Effective Throughput over AWGN Channels

To illustrate the superiority of our proposed modulation scheme more intuitively, Fig. 3 depicts the BER and effective throughput of different modulation schemes over AWGN channels. In particular, to quantize the advantages with respect to the actual throughput achievable by different modulation schemes, the effective throughput T_E (bps) can be defined as [17], [23]

$$T_E = \eta BW(1 - P_b), \tag{32}$$

where η and P_b represent the SE and BER for a given modulation scheme.

On one hand, the EE of our proposed modulation scheme suffers from deterioration due to the layered-and-grouped-multiplexing signal structure, which is reflected in the BER performance degradation. As illustrated in Fig. 3(a), the conventional LoRa modulation achieves the best BER performance, i.e., the highest EE. The performance loss of GCSS modulation and LCSS modulation compared to the conventional LoRa modulation is less than 0.5 dB at a BER
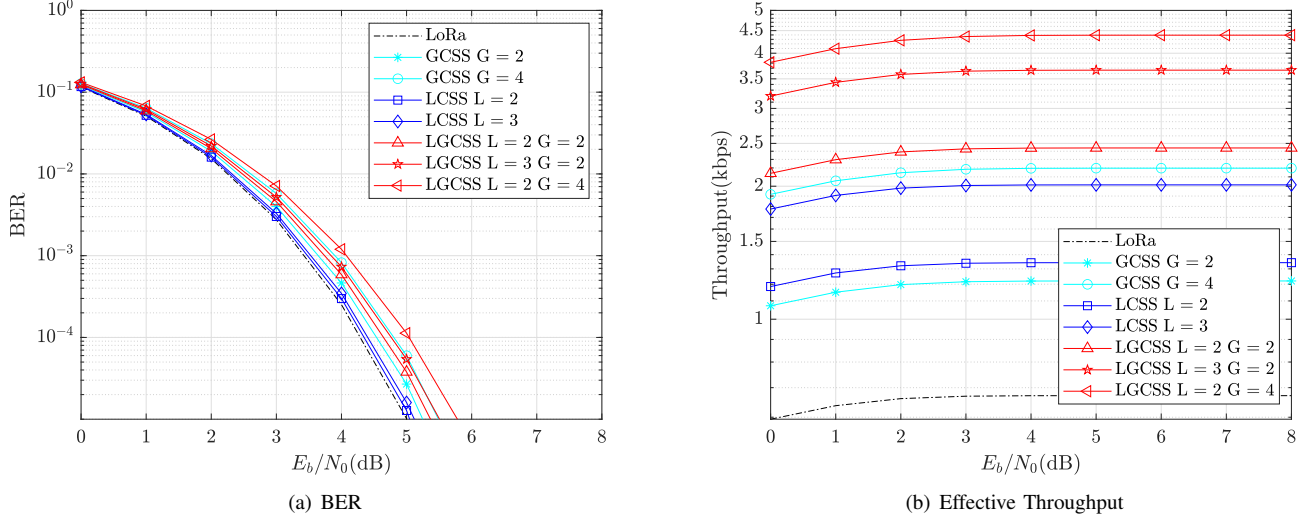
(a) BER

(b) Effective Throughput

Fig. 3. BER and effective throughput of different modulation schemes over AWGN channels for $SF = 11$.
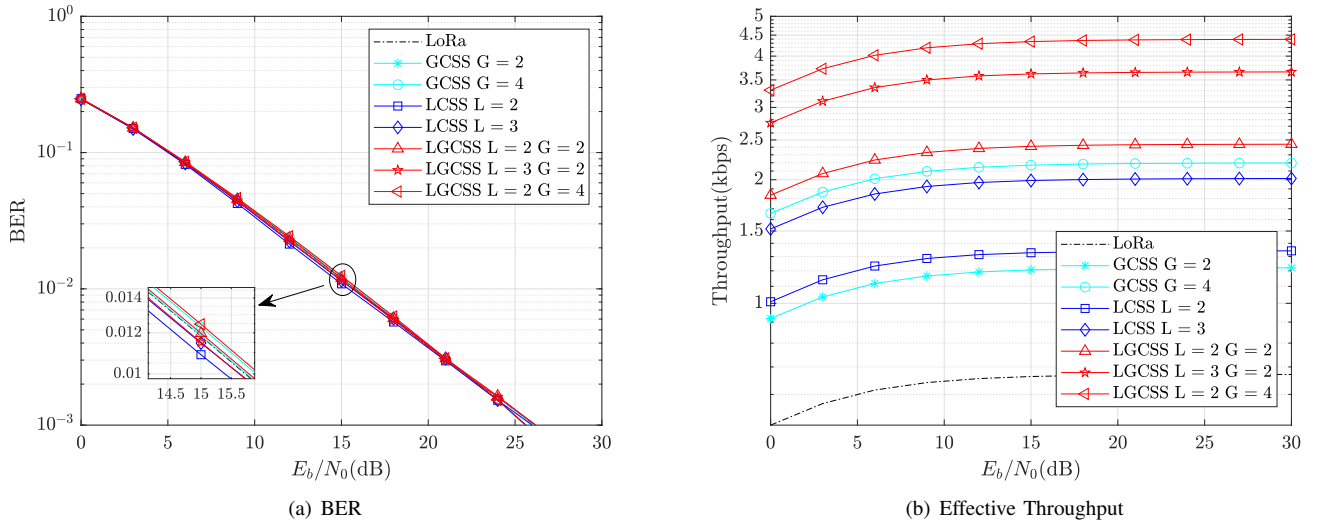

(a) BER

(b) Effective Throughput

Fig. 4. BER and effective throughput of different modulation schemes over Rayleigh fading channels for $SF = 11$.

level of 10^{-5}. However, with the increase of L and G, LGCSS modulation suffers from more severe performance loss relative to the conventional LoRa modulation. Nevertheless, the performance loss of LGCSS modulation is only about 0.8 dB at a BER level of 10^{-5} for $L = 2$ and $G = 4$, which shows that the EE deterioration of our proposed scheme is still acceptable for small L and G.

On the other hand, a salient feature of our proposed LGCSS modulation is that it can achieve much higher SE than its traditional counterparts, which is reflected in the T_E improvements and is one of the key aspects required for massive IoT applications with limited spectrum resources. Fig. 3(b) illustrates that LGCSS modulation achieves a noteworthy performance gain in terms of effective throughput compared to its classical counterparts. Specifically, the effective throughput of LGCSS

modulation is nearly eight times that of the conventional LoRa modulation for $L = 2$ and $G = 4$. Moreover, facilitated by the design parameters of L, G, and M, LGCSS modulation could significantly improve the achievable data rate in a more flexible manner than GCSS modulation and LCSS modulation.

C. BER and Effective Throughput over Rayleigh and Rician Fading Channels

In this subsection, the BER and effective throughput of our proposed LGCSS modulation over both Rayleigh and Rician fading channels are demonstrated. In particular, Fig. 4 presents the BER and effective throughput of different modulation schemes over Rayleigh fading channels which characterizes the performance under a non-line-of-sight (NLoS)
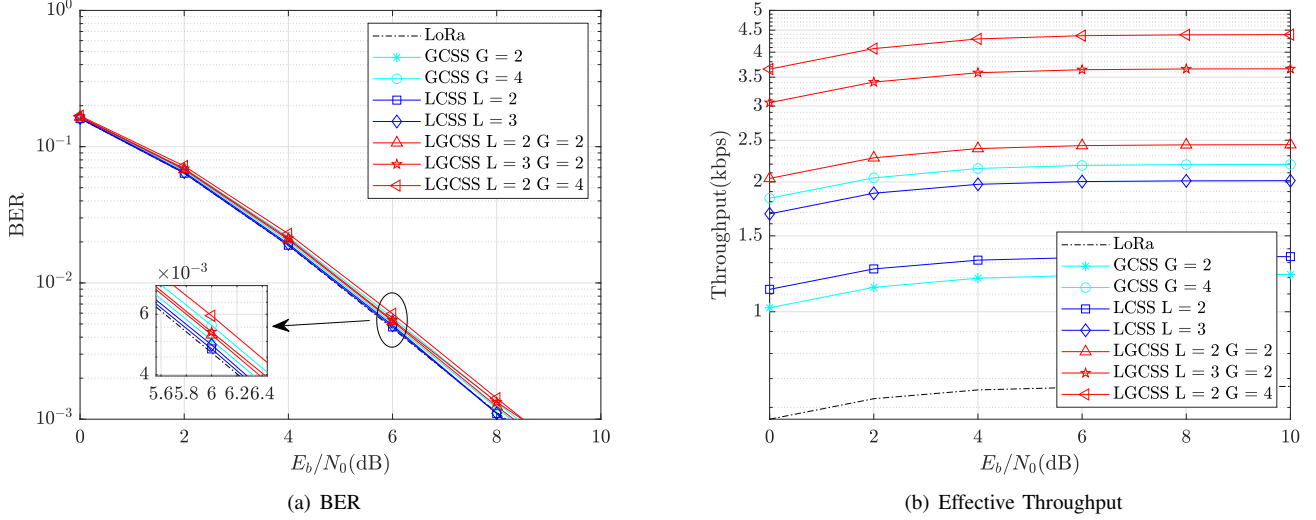
Fig. 5. BER and effective throughput of different modulation schemes over Rician fading channels for $SF = 11$.

environment. Moreover, Fig. 5 presents the BER and effective throughput over Rician fading channels with the Rice factor $K = 10$ which characterizes the performance under a LoS environment. As shown in Fig. 4(a) and Fig. 5(a), the BER curves of different modulation schemes appear very close to each other, which demonstrates that our proposed LGCSS modulation and other classical counterparts have similar EE over both Rayleigh and Rician fading channels. However, by inspecting Fig. 3(a) and Fig. 4(a), it can be observed that the Rayleigh fading results in a considerable BER performance loss, which boils down to the deterioration of EE. Nevertheless, as illustrated in Fig. 4(b) and Fig. 5(b), LGCSS modulation still achieves a significant effective throughput gain compared to the classical counterparts. This comparison validates the superiority of our proposed modulation scheme once again. On one hand, as the link-level data rate increases, the time-on-air (ToA) of a fixed-length packet decreases, which improves the transmission efficiency and reduces the probability of packet collisions, thus enhancing the network scalability [28]. On the other hand, the decreased ToA reduces energy consumption of IoT end devices which are mostly battery-powered and contributes to their long life expectancy [29].

D. BER Performance Under the Impact of Phase Offset

In this subsection, the BER performance of our proposed LGCSS modulation under the impact of phase offset (PO) is investigated. The received signal corrupted by PO is given as

$$r[n] = s[n] \exp\{j\phi\} + w[n], \qquad (33)$$

where ϕ denotes the PO. Herein, Fig. 6 demonstrates the BER performance of LGCSS modulation for $SF = 11$ with PO. It can be observed that the BER performance of LGCSS modulation configured with different L and G in the case of $\phi = \pi/8$ is identical to that of $\phi = 0$, which demonstrates
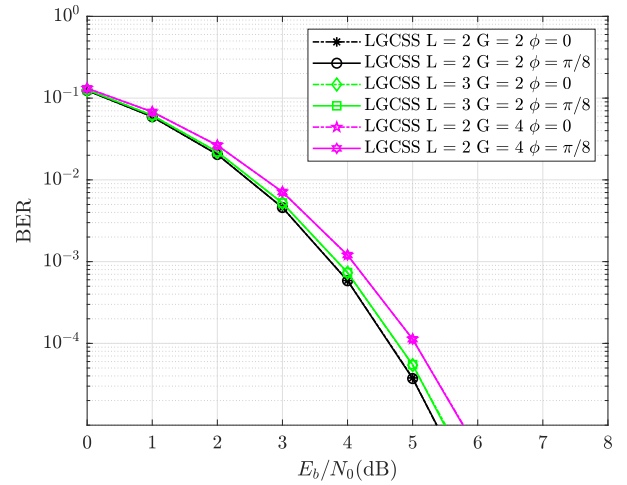

Fig. 6. BER performance of LGCSS modulation for $SF = 11$ with PO.

its robustness against PO due to the employed non-coherent detection.

E. BER Performance Under the Impact of Frequency Offset

In this subsection, the BER performance of LGCSS modulation under the impact of frequency offset (FO) is investigated. The received signal corrupted by FO is given as

$$r[n] = s[n] \exp\{j2\pi\epsilon n/M\} + w[n], \qquad (34)$$

where ϵ denotes the normalized FO. Fig. 7 presents the BER performance of LGCSS modulation for $SF = 11$ with FO. It can be observed that the proposed LGCSS modulation is more severely impacted by FO with the increase of L and G. In particular, as shown in Fig. 7, the BER performance loss is around 0.1 dB, 0.15 dB, and 0.2 dB for LGCSS modulation with $L = 2$ and $G = 2$, LGCSS modulation with $L = 3$
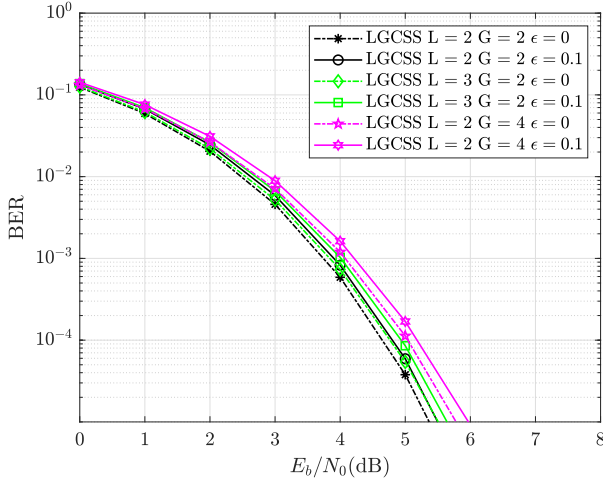
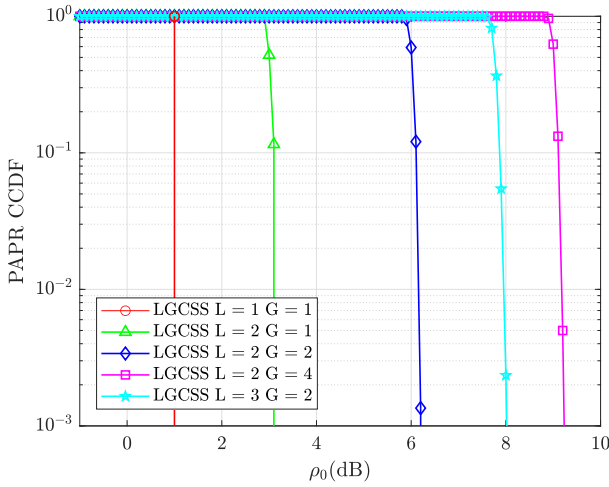Fig. 7. BER performance of LGCSS modulation for $SF = 11$ with FO.

Fig. 8. PAPR CCDF for different variants of LGCSS modulation. The CCDF curves are obtained for $SF = 11$.

and $G = 2$, and LGCSS modulation with $L = 2$ and $G = 4$, respectively, when $\epsilon = 0.1$. Nevertheless, the performance degradation is still acceptable for small ϵ.

F. Peak-to-Average Power Ratio Analysis

Despite the fact that LGCSS modulation is capable of significantly improving the effective throughput compared to the traditional counterparts and achieving a more extensive trade-off between EE and SE, it does not possess a constant envelope property like the conventional LoRa modulation due to the layered-and-grouped-multiplexing signal structure. In general, most SC-CSS modulation schemes show a constant envelope property while MC-CSS modulation schemes have higher peak-to-average power ratio (PAPR) [30]. Specifically, the PAPR of LGCSS modulation signal can be mathematically defined as

$$\rho = \frac{\max_{n} |s[n]|^2}{\frac{1}{M} \sum_{n=0}^{M-1} |s[n]|^2}. \tag{35}$$

By calculating the complementary cumulative distribution function (CCDF) of the PAPR as $\Pr\{\rho > \rho_0\}$, we obtain the numerical results in Fig. 8. It can be observed that the PAPR of LGCSS modulation depends on the configurations of both L and G. Larger L and G could lead to higher PAPR, which is the cost to attain higher SE and enhanced data rate.

G. Future Research Directions

Based on the above discussions, we outline some future research directions related to the CSS-based waveform design in the context of IoT applications.

1) Novel Modulation Schemes: Benefiting from the proposed design framework, it is expected that new CSS-based modulation schemes can be developed to accommodate the ever-increasing application domains. For instance, the Layered FSCSS-IM can be obtained through *inter-layer multiplexing* and *intra-group index combination* with design parameters $(L, 1, M)$. Moreover, the proposed design framework can be combined with other waveform design techniques in the literature such as interleaving [31]–[33], IQ (in-phase and quadrature) multiplexing [17], [34], and phase modulation [35]–[39] to obtain a more extensive trade-off between EE and SE. Developing low-complexity detection methods for such novel modulation schemes also remains to be further investigated.

2) Advanced Channel Coding Schemes: Although Hamming code is currently employed in LoRa PHY layer, more advanced channel coding schemes can be utilized to further enhance the robustness of IoT communications. For example, Turbo code [40], [41] has been proposed to enhance the BER performance of SSK-LoRa modulation and LCSS modulation, respectively. In addition, low-density parity-check (LDPC) code [42] has also been studied in CSS-based communication systems. It is emphasized that a proper forward error correction (FEC) strategy could lead to a more flexible trade-off between EE and SE. This motivates more in-depth study into the appropriate channel coding schemes to be incorporated into various CSS-based LoRa-like modulation schemes.

3) MIMO Extension: Multiple-input multiple-output (MIMO) technology has the outstanding capability to increase effective throughput and improve link reliability. Thus, multiple antenna techniques can provide great potential for CSS-based modulation schemes through time-frequency-spatial domain joint design [43]. For example, by employing space-time block coding (STBC), a MIMO-LoRa system can obtain considerable transmit and receive diversity over fading channels [44]. Moreover, a reconfigurable intelligent surface (RIS) assisted LoRa system has been recently proposed to further increase the achievable throughput [45]. As such, it is quite important to make a compelling trade-off between multiplexing and diversity under the analytical framework of MIMO-CSS to fulfill the practical requirements of heterogeneous application domains.

V. CONCLUSION

In this paper, we formulated a unified framework for the CSS-based waveform design and proposed a novel LGCSS

modulation scheme which can achieve much higher SE and better flexibility than its traditional counterparts. The complete transceiver architecture of our proposed scheme was presented along with both coherent and non-coherent detection methods. Moreover, a comprehensive performance analysis was conducted in terms of orthogonality, BEP, and computational complexity. Numerical results not only validate the accuracy of our theoretical analysis but also demonstrate substantial performance improvements of our proposed modulation scheme in terms of effective throughput. In a word, the proposed modulation scheme can be considered as a promising candidate to satisfy the ever-increasing demands of heterogeneous IoT applications. Furthermore, the presented waveform design framework is also expected to inspire new future research in this field.

APPENDIX A
DERIVATIONS OF (18)

The generalized quadratic Gauss sum can be expressed as

$$G(a, b, c) = \sum_{n=0}^{|c|-1} \exp\left\{ j\frac{\pi}{c}(an^2 + bn) \right\}, \qquad (36)$$

where a, b, c are integers with $ac \neq 0$ and $ac + b$ is even. According to the reciprocity theorem for Gauss sums [46], (36) can be simplified as

$$G(a, b, c) = \sqrt{\left|\frac{c}{a}\right|} \exp\left\{ j\frac{\pi}{4ac}(|ac| - b^2) \right\}$$
$$\sum_{n=0}^{|a|-1} \exp\left\{ -j\frac{\pi}{a}(bn + cn^2) \right\}. \qquad (37)$$

Therefore, for $I_{m_g^l, \widetilde{m}_{\widetilde{g}}^{\widetilde{l}}}^{l, \widetilde{l}}$ we have $a = \alpha_{(l, \widetilde{l})}$, $b = 2\beta_{(m_g^l, \widetilde{m}_{\widetilde{g}}^{\widetilde{l}})}$, $c = M$ and it can be further derived as

$$I_{m_g^l, \widetilde{m}_{\widetilde{g}}^{\widetilde{l}}}^{l, \widetilde{l}} = \sum_{n=0}^{M-1} \exp\left\{ j\frac{\pi}{M}[\alpha_{(l, \widetilde{l})} n^2 + 2\beta_{(m_g^l, \widetilde{m}_{\widetilde{g}}^{\widetilde{l}})} n] \right\}$$
$$= \sqrt{\frac{M}{|\alpha_{(l, \widetilde{l})}|}} \mathcal{A}_{(l, \widetilde{l})} (1 + \mathcal{B}_{(m_g^l, \widetilde{m}_{\widetilde{g}}^{\widetilde{l}})}), \qquad (38)$$

where

$$\mathcal{A}_{(l, \widetilde{l})} = \exp\left\{ j\frac{\pi |\alpha_{(l, \widetilde{l})}|}{4\alpha_{(l, \widetilde{l})}} \right\} \exp\left\{ -j\frac{\pi \beta_{(m_g^l, \widetilde{m}_{\widetilde{g}}^{\widetilde{l}})}^2}{\alpha_{(l, \widetilde{l})} M} \right\}, \qquad (39)$$

$$\mathcal{B}_{(m_g^l, \widetilde{m}_{\widetilde{g}}^{\widetilde{l}})} = \sum_{n=1}^{|\alpha_{(l, \widetilde{l})}|-1} \exp\left\{ -j\frac{\pi}{\alpha_{(l, \widetilde{l})}}[Mn^2 + 2\beta_{(m_g^l, \widetilde{m}_{\widetilde{g}}^{\widetilde{l}})} n] \right\}. \qquad (40)$$

APPENDIX B
DERIVATIONS OF (29)

For GCSS modulation, the received signal over AWGN channel is given in [19]

$$r[n] = \frac{1}{\sqrt{G}} \sum_{g=1}^{G} c_1[n] \exp\left\{ j\frac{2\pi m_g^1 n}{M} \right\} + w[n], \qquad (41)$$

where $c_1[n] = \frac{1}{\sqrt{M}} \exp\left\{ j\frac{\pi n^2}{M} \right\}$ and $w[n] \sim \mathcal{CN}(0, \sigma^2)$. As such, the dechirped signal $r_1[n]$ is given by

$$r_1[n] = r[n] c_1^*[n]$$
$$= \frac{1}{\sqrt{G}M} \sum_{g=1}^{G} \exp\left\{ j\frac{2\pi m_g^1 n}{M} \right\} + \bar{w}[n], \qquad (42)$$

where $\bar{w}[n] = w[n] c_1^*[n] \sim \mathcal{CN}(0, \frac{\sigma^2}{M})$. Hence, the M-point DFT of the dechirped signal is given by

$$R_1[k] = \frac{1}{\sqrt{G}} \sum_{g=1}^{G} \delta[k - m_g^1] + \bar{W}[k], \qquad (43)$$

where $\bar{W}[k] \sim \mathcal{CN}(0, \sigma^2)$. Therefore, the SEP of GCSS modulation can be formulated as

$$P_G^s = \Pr\left\{ \bigcup_{g=1}^{G} \{\hat{m}_g^1 \neq m_g^1\} \right\} = 1 - \Pr\left\{ \bigcap_{g=1}^{G} \{\hat{m}_g^1 = m_g^1\} \right\}$$
$$\overset{(a)}{=} 1 - [1 - \Pr\{\hat{m}_g^1 \neq m_g^1\}]^G, \forall g \in \{1, ..., G\} \qquad (44)$$

where (a) follows from the fact that the symbol decision is performed separately for each independent group. Consequently, we only need to consider the symbol and bit error probability of one independent group.

Without loss of generality, we take the first group for analysis. Considering non-coherent detection, its symbol decision metric can be expressed as

$$|R_1[k]| = \begin{cases} \left| \frac{1}{\sqrt{G}} + \bar{W}[m_1^1] \right|, & \text{if } k = m_1^1 \\ |\bar{W}[k]|, & \text{otherwise.} \end{cases} \qquad (45)$$

Let us define $\mu = \left| \frac{1}{\sqrt{G}} + \bar{W}[m_1^1] \right|$ which follows the Rician distribution with the shape parameter $K = \frac{1}{G\sigma^2} = \frac{\gamma_s}{G}$, and $\tau_k = |\bar{W}[k]|$ which follows the Rayleigh distribution with CDF expressed as

$$F_{\tau_k}(\tau) = 1 - \exp\left(-\frac{\tau^2}{\sigma^2} \right). \qquad (46)$$

Let $U = \mu$ and $V = \max_{k, k \neq m_1^1}(\tau_k)$ denote a random variable for the maximum of $\frac{M}{G} - 1$ independent and identically distributed (i.i.d.) Rayleigh random variables. Since U and V are independent, their joint CDF and joint PDF can be expressed as $F(u, v) = F_U(u) F_V(v)$, $f(u, v) = f_U(u) f_V(v)$, respectively. As such, the SEP of the first group can be given as

$$\Pr\{\hat{m}_1^1 \neq m_1^1\} = \iint_{U < V} f(u, v) du dv$$
$$= \int_0^{\infty} f_U(u) [1 - F_V(u)] du, \qquad (47)$$

where

$$F_V(u) = \Pr\{V \leq u\} = \Pr\left\{ \max_{k, k \neq m_1^1}(\tau_k) \leq u \right\}$$
$$= \left[1 - \exp\left(-\frac{u^2}{\sigma^2} \right) \right]^{\frac{M}{G}-1}, \qquad (48)$$

$$f_U(u) = \frac{2u}{\sigma^2} \exp\left\{-\frac{u^2 + \frac{1}{G}}{\sigma^2}\right\} I_0\left(\frac{\frac{2u}{\sqrt{G}}}{\sigma^2}\right), \qquad (49)$$

with $I_0(\cdot)$ denoting the modified zero-order Bessel function of the first kind.

Let $p_1^1 = \Pr\{\hat{m}_1^1 \neq m_1^1\}$, (47) can be formulated as

$$
\begin{aligned}
p_1^1 &= \int_0^\infty \left\{1 - \left[1 - \exp\left(-\frac{u^2}{\sigma^2}\right)\right]^{\frac{M}{G}-1}\right\} \\
&\quad \times \frac{2u}{\sigma^2} \exp\left\{-\frac{u^2 + \frac{1}{G}}{\sigma^2}\right\} I_0\left(\frac{\frac{2u}{\sqrt{G}}}{\sigma^2}\right) du.
\end{aligned}
\tag{50}
$$

Using the Newton's binomial identity, we have

$$1 - (1 - e^x)^N = \sum_{k=1}^N \binom{N}{k}(-1)^{k+1} e^{xk}. \tag{51}$$

Therefore, (50) can be further simplified as

$$
\begin{aligned}
p_1^1 &= \sum_{k=1}^{\frac{M}{G}-1} (-1)^{k+1} \binom{\frac{M}{G}-1}{k} \int_0^\infty \exp\left\{-\frac{ku^2}{\sigma^2}\right\} \\
&\quad \times \frac{2u}{\sigma^2} \exp\left\{-\frac{u^2 + \frac{1}{G}}{\sigma^2}\right\} I_0\left(\frac{\frac{2u}{\sqrt{G}}}{\sigma^2}\right) du \\
&= \sum_{k=1}^{\frac{M}{G}-1} (-1)^{k+1} \binom{\frac{M}{G}-1}{k} \exp\left\{-\frac{k}{k+1}\frac{\frac{1}{G}}{\sigma^2}\right\} \\
&\quad \times \int_0^\infty \frac{2u}{\sigma^2} \exp\left\{-\frac{(k+1)u^2 + \frac{\frac{1}{G}}{k+1}}{\sigma^2}\right\} I_0\left(\frac{\frac{2u}{\sqrt{G}}}{\sigma^2}\right) du.
\end{aligned}
\tag{52}
$$

Since the integral in (52) can be computed as

$$\int_0^\infty \frac{2u}{\sigma^2} \exp\left\{-\frac{(k+1)u^2 + \frac{\frac{1}{G}}{k+1}}{\sigma^2}\right\} I_0\left(\frac{\frac{2u}{\sqrt{G}}}{\sigma^2}\right) du = \frac{1}{k+1}, \tag{53}$$

we have

$$
\begin{aligned}
p_1^1 &= \sum_{k=1}^{\frac{M}{G}-1} \frac{(-1)^{k+1}}{k+1} \binom{\frac{M}{G}-1}{k} \exp\left\{-\frac{k}{k+1}\frac{\gamma_s}{G}\right\} \\
&= P_L^s\left(\frac{M}{G}, \frac{\gamma_s}{G}\right).
\end{aligned}
\tag{54}
$$

Hence, the closed-form BEP expression for GCSS modulation can be expressed as

$$P_G^b = \frac{M}{2(M-G)} P_L^s\left(\frac{M}{G}, \frac{\gamma_s}{G}\right). \tag{55}$$

REFERENCES

[1] D. C. Nguyen et al., "6G Internet of Things: A Comprehensive Survey," *IEEE Internet Things J.*, vol. 9, no. 1, pp. 359-383, Jan. 2022.

[2] K. L. Lueth. "State of the IoT 2020: 12 Billion IoT Connections, Surpassing Non-IoT for the First Time." 2020. [Online]. Available: https://iot-analytics.com/

[3] U. Raza, P. Kulkarni and M. Sooriyabandara, "Low Power Wide Area Networks: An Overview," *IEEE Commun. Surveys Tuts.*, vol. 19, no. 2, pp. 855-873, 2rd Quart., 2017.

[4] M. Kanj, V. Savaux and M. Le Guen, "A Tutorial on NB-IoT Physical Layer Design," *IEEE Commun. Surveys Tuts.*, vol. 22, no. 4, pp. 2408-2446, 4th Quart., 2020.

[5] J. P. Shanmuga Sundaram, W. Du and Z. Zhao, "A Survey on LoRa Networking: Research Problems, Current Solutions, and Open Issues," *IEEE Commun. Surveys Tuts.*, vol. 22, no. 1, pp. 371-388, 1st Quart., 2020.

[6] LoRa Alliance. Accessed: Sept. 2023. [Online]. Available: https://lora-alliance.org/

[7] R. Marini, K. Mikhaylov, G. Pasolini and C. Buratti, "Low-Power Wide-Area Networks: Comparison of LoRaWAN and NB-IoT Performance," *IEEE Internet Things J.*, vol. 9, no. 21, pp. 21051-21063, Nov. 2022.

[8] G. Baruffa, L. Rugini, V. Mecarelli, L. Germani and F. Frescura, "Coded LoRa performance in wireless channels," in *Proc. IEEE Annu. Int. Symp. Pers. Indoor Mobile Radio Commun. (PIMRC)*, Sep. 2019, pp. 1-6.

[9] G. Pasolini, "On the LoRa Chirp Spread Spectrum Modulation: Signal Properties and Their Impact on Transmitter and Receiver Architectures," *IEEE Trans. Wireless Commun.*, vol. 21, no. 1, pp. 357-369, Jan. 2022.

[10] W. Xu et al., "The Design, Implementation, and Deployment of a Smart Lighting System for Smart Buildings," *IEEE Internet Things J.*, vol. 6, no. 4, pp. 7266-7281, Aug. 2019.

[11] A. Staikopoulos, V. Kanakaris and G. A. Papakostas, "Image Transmission via LoRa Networks – A Survey," in *Proc. IEEE Int. Conf. Image, Vis. Comput.*, Beijing, China, 2020, pp. 150-154.

[12] D. Magrin, M. Capuzzo, A. Zanella, L. Vangelista and M. Zorzi, "Performance Analysis of LoRaWAN in Industrial Scenarios," *IEEE Trans. Ind. Informat.*, vol. 17, no. 9, pp. 6241-6250, Sept. 2021.

[13] H. H. R. Sherazi, L. A. Grieco, M. A. Imran and G. Boggia, "Energy-Efficient LoRaWAN for Industry 4.0 Applications," *IEEE Trans. Ind. Informat.*, vol. 17, no. 2, pp. 891-902, Feb. 2021.

[14] A. W. Azim, A. Bazzi, R. Shubair, and M. Chafii. *A Survey on Chirp Spread Spectrum-based Waveform Design for IoT.* [Online]. Available: https://arxiv.org/abs/2208.10274

[15] L. Vangelista, "Frequency Shift Chirp Modulation: The LoRa Modulation," *IEEE Signal Process. Lett.*, vol. 24, no. 12, pp. 1818-1821, Dec. 2017.

[16] M. Hanif and H. H. Nguyen, "Slope-shift keying LoRa-based modulation," *IEEE Internet Things J.*, vol. 8, no. 1, pp. 211-221, Jan. 2021.

[17] I. Bizon Franco de Almeida, M. Chafii, A. Nimr and G. Fettweis, "Alternative Chirp Spread Spectrum Techniques for LPWANs," *IEEE Trans. Green Commun. Netw.*, vol. 5, no. 4, pp. 1846-1855, Dec. 2021.

[18] L. Vangelista and A. Cattapan, "A new LoRa-compatible modulation improving the LoRaWAN network level performance," in *Proc. IEEE Latin-Amer. Conf. Commun. (LATINCOM)*, 2019, pp. 1-6.

[19] Q. Yu, H. Wang, Z. Lu and S. An, "Group-Based CSS Modulation: A Novel Enhancement to LoRa Physical Layer," *IEEE Wireless Commun. Lett.*, vol. 11, no. 3, pp. 660-664, Mar. 2022.

[20] S. An, H. Wang, Y. Sun, Z. Lu and Q. Yu, "Time Domain Multiplexed LoRa Modulation Waveform Design for IoT Communication," *IEEE Commun. Lett.*, vol. 26, no. 4, pp. 838-842, Apr. 2022.

[21] A. W. Azim, A. Bazzi, M. Fatima, R. Shubair and M. Chafii, "Dual-Mode Time Domain Multiplexed Chirp Spread Spectrum," *IEEE Trans. Veh. Technol.*, early access.

[22] M. Hanif and H. H. Nguyen, "Frequency-Shift Chirp Spread Spectrum Communications With Index Modulation," *IEEE Internet Things J.*, vol. 8, no. 24, pp. 17611-17621, Dec. 2021.

[23] H. Ma, Y. Fang, G. Cai, G. Han and Y. Li, "A New Frequency-Bin-Index LoRa System for High-Data-Rate Transmission: Design and Performance Analysis," *IEEE Internet Things J.*, vol. 9, no. 14, pp. 12515-12528, Jul. 2022.

[24] A. W. Azim, A. Bazzi, R. Bomfin, R. Shubair and M. Chafii, "Layered Chirp Spread Spectrum Modulations for LPWANs," *IEEE Trans. Commun.*, early access.

[25] A. Goldsmith. *Wireless Communications.* Cambridge University Press, 2005.

[26] T. Elshabrawy and J. Robert, "Closed-form approximation of LoRa modulation BER performance," *IEEE Commun. Lett.*, vol. 22, no. 9, pp. 1778-1781, Sep. 2018.

[27] G. Baruffa and L. Rugini, "Performance of LoRa-Based Schemes and Quadrature Chirp Index Modulation," *IEEE Internet Things J.*, vol. 9, no. 10, pp. 7759-7772, May 15, 2022.

[28] Y. Bouazizi, F. Benkhelifa, H. ElSawy and J. A. McCann, "On the Scalability of Duty-Cycled LoRa Networks With Imperfect SF Orthogonality," *IEEE Wireless Commun. Lett.*, vol. 11, no. 11, pp. 2310-2314, Nov. 2022.

[29] A. Petroni and M. Biagi, "Interference Mitigation and Decoding Through Gateway Diversity in LoRaWAN," *IEEE Trans. Wireless Commun.*, vol. 21, no. 11, pp. 9068-9081, Nov. 2022.

[30] A. W. Azim, R. Shubair and M. Chafii, "Chirp Spread Spectrum-based Waveform Design and Detection Mechanisms for LPWAN-based IoT – A Survey," *IEEE Access*, early access.

[31] T. Elshabrawy and J. Robert, "Interleaved Chirp Spreading LoRa-Based Modulation," *IEEE Internet Things J.*, vol. 6, no. 2, pp. 3855-3863, Apr. 2019.

[32] Y. Shi, W. Xu and L. Wang, "An Enhanced Interleaved Chirp Spreading LoRa Modulation Scheme for High Data Transmission," in *Proc. 2022 Wireless Telecommunications Symposium (WTS)*, 2022, pp. 1-6.

[33] A. Mondal, M. Hanif and H. H. Nguyen, "SSK-ICS LoRa: A LoRa-Based Modulation Scheme With Constant Envelope and Enhanced Data Rate," *IEEE Commun. Lett.*, vol. 26, no. 5, pp. 1185-1189, May 2022.

[34] I. B. F. de Almeida, M. Chafii, A. Nimr and G. Fettweis, "In-phase and quadrature chirp spread spectrum for IoT communications," in *Proc. IEEE Global Commun. Conf. (GLOBECOM)*, Taipei, Taiwan, Dec. 2020, pp. 1-6.

[35] R. Bomfin, M. Chafii and G. Fettweis, "A novel modulation for IoT: PSK-LoRa," in *Proc. IEEE Veh. Technol. Conf.*, Apr. 2019, pp. 1-5.

[36] T. T. Nguyen, H. H. Nguyen, R. Barton and P. Grossetete, "Efficient Design of Chirp Spread Spectrum Modulation for Low-Power Wide-Area Networks," *IEEE Internet Things J.*, vol. 6, no. 6, pp. 9503-9515, Dec. 2019.

[37] A. W. Azim, J. L. G. Monsalve and M. Chafii, "Enhanced PSK-LoRa," *IEEE Wireless Commun. Lett.*, vol. 11, no. 3, pp. 612-616, Mar. 2022.

[38] X. Yu, X. Cai, W. Xu, H. Sun and L. Wang, "Differential Phase Shift Keying-Aided Multi-Mode Chirp Spread Spectrum Modulation," *IEEE Wireless Commun. Lett.*, vol. 13, no. 2, pp. 298-302, Feb. 2024.

[39] Q. Yu, D. He, Z. Lu and H. Wang, "SSK-Based PSK-LoRa Modulation for IoT Communications," *IEEE Open J. Commun. Soc.*, vol. 4, pp. 1487-1498, 2023.

[40] S. An, Z. Lu, H. Wang and Q. Yu, "A Turbo Coded LoRa-Index Modulation Scheme for IoT Communication," in *Proc. IEEE 21st Int. Conf. Commun. Technol.*, Tianjin, China, 2021, pp. 736-740.

[41] J. Luo, Y. Bai, B. Bai, C. Chen and W. Wen, "A Multi-layer Superposition Modulation Scheme to Improve the Data Rate for IoT Communications," in *Proc. IEEE/CIC Int. Conf. Commun. Workshops China (ICCC Workshops)*, Dalian, China, 2023, pp. 1-6.

[42] J. Bourduge, C. Poulliat, B. Gadat and J. F. Chouteau, "Bit interleaved chirp spread spectrum coded modulations with iterative decoding based on LDPC codes for coherent and non-coherent regimes," in *Proc. IEEE 33rd Annu. Int. Symp. Pers., Indoor Mobile Radio Commun. (PIMRC)*, Kyoto, Japan, 2022, pp. 968-974.

[43] J. -M. Kang, "MIMO-LoRa for High-Data-Rate IoT: Concept and Precoding Design," *IEEE Internet Things J.*, vol. 9, no. 12, pp. 10368-10369, Jun. 2022.

[44] H. Ma, G. Cai, Y. Fang, P. Chen and G. Han, "Design and Performance Analysis of a New STBC-MIMO LoRa System," *IEEE Trans. Commun.*, vol. 69, no. 9, pp. 5744-5757, Sept. 2021.

[45] X. Zhang, W. Xu, G. Cai, Y. Song and G. Chen, "A New Reconfigurable Intelligent-Surface-Assisted LoRa System," *IEEE Trans. Veh. Technol.*, vol. 71, no. 8, pp. 9055-9060, Aug. 2022.

[46] B. C. Berndt, K. S. Williams, and R. J. Evans. Gauss and Jacobi Sums. 1998.